TSINGHUA SCIENCE AND TECHNOLOGY
ISSN 1007-0214 11/11 pp435–446
DOI: 10.26599/TST.2019.9010028
Volume 25, Number 3, June 2020

Studying the Effect of the Pre-Stimulation Paradigm on Steady-State Visual Evoked Potentials with Dynamic Models Based on the Zero-Pole Analytical Method

Shangen Zhang, Xu Han, and Xiaorong Gao*

Abstract: This study explored methods for improving the performance of Steady-State Visual Evoked Potential (SSVEP)-based Brain-Computer Interfaces (BCI), and introduced a new analytical method to quantitatively analyze and reflect the characteristics of SSVEP. We focused on the effect of the pre-stimulation paradigm on the SSVEP dynamic models and the dynamic response process of SSVEP, and performed a comparative analysis of three pre-stimulus paradigms (black, gray, and white). Four dynamic models with different orders (second- and third-order) and with and without a zero point were used to fit the SSVEP envelope. The zero-pole analytical method was adopted to conduct quantitative analysis on the dynamic models, and the response characteristics of SSVEP were represented by zero-pole distribution characteristics. The results of this study indicated that the pre-stimulation paradigm affects the characteristics of SSVEP, and the dynamic models had good fitting abilities with SSVEPs under various types of pre-stimulation. Furthermore, the zero-pole characteristics of the models effectively characterize the damping coefficient, oscillation period, and other SSVEP characteristics. The comparison of zeros and poles indicated that the gray pre-stimulation condition corresponds to a lower damping coefficient, thus showing its potential to improve the performance of SSVEP-BCIs.

Key words: Steady-State Visual Evoked Potential (SSVEP); dynamic model; pre-stimulation; zero and pole analysis; brain-computer interface

1 Introduction

Steady-State Visual Evoked Potential (SSVEP) is a periodic stable voltage pattern evoked by continuous visual stimulus at a constant frequency that rises mainly in the visual cortex[1,2]. At present, SSVEPs are mainly applied in the Brain-Computer Interface (BCI) field, which are called SSVEP-BCIs[3,4]. SSVEP-BCIs belong to the electroencephalography (EEG)-based BCI systems, which also include Mental Imagery-based BCIs (MI-BCIs) and P300-BCIs[5,6]. In addition, speech decoding BCIs also recently become a focus of research[7–9]. In traditional SSVEP-BCIs, a target would be determined by identifying the SSVEP frequency as each target flickers with a specified frequency[10–12]. These stimuli frequencies would utilize low-frequency (<15 Hz), medium-frequency ($15-30$ Hz), or high-frequency bands (>30 Hz)[13–15], among which the low frequency band was the most commonly used.

With the improvement in visual stimulus coding methods and target recognition algorithms, SSVEP-BCI has made significant progress. Previous studies have shown that SSVEP characteristics are highly related with the physical properties of visual stimuli, such as frequency, phase, brightness, and contrast[16–18]. Over

• Shangen Zhang, Xu Han, and Xiaorong Gao are with the Department of Biomedical Engineering, School of Medicine, Tsinghua University, Beijing 100084, China. E-mail: zhangsfphd@163.com; hanxu29@163.com; gxr-dea@tsinghua.edu.cn.

* To whom correspondence should be addressed.

Manuscript received: 2019-06-21; revised: 2019-07-18; accepted: 2019-08-01

recent decades scholars have mainly focused on the physical properties of SSVEP stimulation[1, 12], while neglecting the effect of the physical properties of visual stimulation outside of the SSVEP stimulation time. However, pre-stimulation, which is the brightness of stimulation prior to SSVEP presentation, may also affect SSVEP characteristics.

Pre-stimulation is therefore a little-studied stimulus paradigm that has the potential to alter SSVEP characteristics. Pre-stimulation at different levels of brightness affects the physical properties of visual stimulation before SSVEP stimulation, and may further affect the initial state of the brain. Pre-stimulation may also affect the brain's allocation of attention resources. The transition from pre-stimulation to SSVEP stimulation will lead to an Event-Related Potential (ERP). Since EEG in the transition process is a mix of ERP and SSVEP signals, the characteristics of ERP will inevitably affect the allocation of attention resources, and therefore affect the SSVEP. However, there have been few studies on pre-stimulation, and an exploration of the relationship between pre-stimulation and SSVEP may help us to improve the performance of SSVEP-BCI. The purpose of the present study is to explore the effect of pre-stimulation on SSVEP, and further explore the potential to improve SSVEP-BCI with a pre-stimulation method. This study focused on the effect of pre-stimulation on the SSVEP dynamic process, used four dynamic models to quantitatively measure the dynamic change process of SSVEP, and evaluated the effect of pre-stimulation on SSVEP by means of a zero-pole analysis.

In order to verify the effect of pre-stimulation properties on SSVEP characteristics, the method of dynamic modeling was used in this study. Many methods have been used to analyze SSVEP characteristics, among which a dynamic model method is an effective tool. The dynamic process of SSVEP is the process of change in SSVEP after the onset of periodic visual stimulation, and the dynamic model is the mathematical model used to simulate this dynamic process. It is known that frequency, phase, and amplitude are the main attributes of SSVEP, of which the amplitude characteristics directly reflect the response intensity of SSVEP, and have a direct impact on the identification accuracy of an SSVEP-BCI system. Therefore, it is of great significance to analyze the response process of SSVEP amplitude, which is the dynamic process of the SSVEP envelope. Previous studies have shown that the dynamic response process of SSVEP can be divided into the Transient-State Response (TSR) and Steady-State Response (SSR)[19–21]. The transient process lasts about 0.5 s, in which the amplitude and phase of SSVEP are unstable[22], while the steady-state response process has the characteristics of stability in amplitude and phase[22, 23]. With the progress of data processing technology and the pursuit of a high Information Transfer Rate (ITR) in SSVEP-BCI research, the length of SSVEP data used for target recognition is becoming shorter and shorter, and the transient process of SSVEP is playing an increasingly important role[12, 24]. However, due to the characteristics instability of transient processes, the quantitative description of the SSVEP envelope and the analysis of SSVEP characteristics have become more challenging. A dynamic modeling method, which adopts the dynamic models to fit the SSVEP envelope, provides an effective quantitative method for the analysis of the dynamic characteristics of SSVEP.

In fact, the dynamic modeling method has been used recently in the study of SSVEP characteristics due to its advantages in quantitative analysis and signal characterization. One typical example of studying SSVEP characteristics with a signal model was discussed in Ref. [25], in which a second-order zero-free model was used to fit the SSVEP envelope. The SSVEP characteristics were represented by model parameters with specific physical and physiological significances. Different from Ref. [25], in which the dynamic model was used to describe the response of the SSVEP envelope, the present study attempts to evaluate the signal channel with a zero-pole analysis, so as to better extract the effective characteristics of SSVEP. This study compared the results of this zero-pole method with the parametric method used in Ref. [25], and analyzed how the advantages of the zero-pole method were reflected in the results of the comparison.

The zero-pole analytical method, which is an intuitive method of analysis for dynamic models, was used in this study to compare different pre-stimulation conditions. The SSVEP response characteristics can be quantitatively reflected by the features of zeros and poles. The Laplace transform transforms the time domain function into a function of the complex frequency variable s, with the complex frequency domain named the s-domain[26, 27].

Generally speaking, the poles of the system determine the intrinsic characteristics of the system, while the zeros have a great influence on the transient response of the system[27]. Poles directly reflect information

related to the stability of a system: a causal system is stable only if all of the poles are located in the left plane of the s-domain[26]. In addition, the real and imaginary coordinates of conjugate poles are related to the damping coefficient and oscillation frequency, respectively. Meanwhile, zeros may affect the amplitude and phase of the waveforms[28]. Different from zero-pole analysis, the method of model parameter analysis is now only used for ultra-low-order (e.g., second-order) systems to avoid the difficulty of interpreting the meanings of parameters in complex models, although higher-order systems may further improve the fitting accuracy in practice. The advantage of this method is that, without needing to explain the exact meaning of the model parameters, the zero-pole analytical method interprets the system properties by the zero-pole characteristic, so as to achieve the combination of a high fitting accuracy of the higher order model and the analyzability of the signal.

This study used the same SSVEP data as that in Ref. [25]. Two frequencies (9 Hz and 15 Hz) were chosen as the stimulation frequencies near the alpha band, around which the inducement of a higher SNR of SSVEP had been shown[14, 29]. The EEG experiments were designed based on these two stimulus frequencies (9 Hz and 15 Hz), two initial phases (0 and π), three levels of pre-stimulation (black, gray, and white), and used the multi-phase processing method to obtain SSVEPs. Four models were used to fit SSVEP envelopes: second-order without zero point (Model 1), second-order with zero point (Model 2), third-order without zero point (Model 3), and third-order with zero point (Model 4). In order to verify the effectiveness of the zero-pole analytical method, we analyzed the zero-pole characteristics of the four models based on the SSVEP envelope data corresponding to the three kinds of pre-stimulation. The fitting results of the four models with SSVEP envelopes were compared, by which the effects of model order and zero point to the fitting results were analyzed. Moreover, we compared the zero-pole characteristics between the three kinds of pre-stimulation in an attempt to identify the optimal pre-stimulation method for SSVEP-BCI performance.

2 Materials and Methods

2.1 Experimental design

Each subject participated in 9 blocks of the EEG experiment. Each block was made up of 48 trials (3 pre-stimulations $\times$2 frequencies $\times$2 phases $\times$4 repetitions) and 10 key tasks, which were presented in random order. Each trial lasted for 4 s. The key tasks were used to improve the subject's attention, and required pressing the space bar as soon as possible. Once the space bar was pressed, the program would move to the next trial. Each trial started with a blank for 1 s with a cross mark on the center of the screen. Subjects were allowed to blink and then shift their gaze to the target as soon as possible within this blank period. After the blank offset, a pre-stimulus square (black, gray, or white) appeared on the screen and remained for 1 s. Following this pre-stimulus offset, a sinusoidal stimulus began to flicker and lasted for 2 s. There was a rest time between blocks, each of which lasted about 5 minutes, and the duration of the whole experimental process was about 2 hours. The experiment design is shown in Fig. 1.

A 23.6-inch Liquid-Crystal Display (LCD) screen with a resolution of 1920 pixel $\times$ 1080 pixel and a refresh rate of 60 Hz was used to present the visual stimulation. The stimulus (including pre-stimuli and SSVEP stimuli) was rendered within a 250 pixel $\times$ 250 pixel square in the center of the screen. The screen area surrounding the stimulus was black. Pre-stimuli conditions could be black (RGB (0, 0, 0)), gray (RGB (128, 128, 128)), or white (RGB (255, 255, 255)) by luminance. In the SSVEP stimuli condition, the sampled sinusoidal stimulation method[30, 31] was used to present visual flickers. Generally, the sequence $s(f,i)$, corresponding to frequency f and frame i, can be generated by

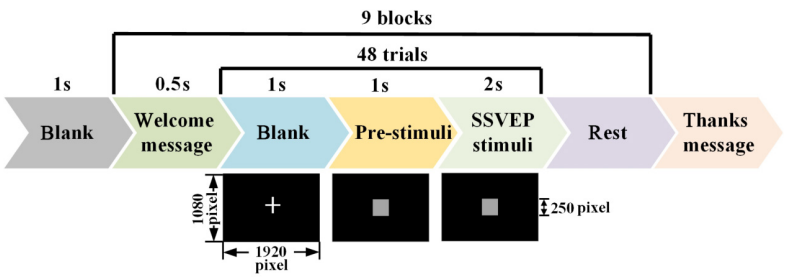

Fig. 1 Parameters setting of stimulus paradigm.

modulating the luminance of the screen using the following Eq. (1),

$$s(f,i)=\frac{1}{2}\left[1+\sin\left[2\pi f\left(\frac{i}{\text{RefreshRate}}+\phi\right)\right]\right] \quad (1)$$

In this study, the frequency f was 9 Hz or 15 Hz, the RefreshRate was 60 Hz, ϕ could be 0 or π (the two opposite initial phases), and the dynamic range of the stimulation signal ranged from 0 (RGB(0, 0, 0)) to 1 (RGB(255, 255, 255)).

2.2 Data acquisition

Fourteen subjects participated in this study, made up of 5 females and 9 males, aged $18-31$ years (mean age is 25 years), with normal or corrected-to-normal vision. Each subject signed his or her written informed consent before the experiment and was paid for his or her participation. This study was approved by the Research Ethics Committee of Tsinghua University.

A Neuroscan SynAmps2 amplifier was used to acquire the EEG data at a sampling rate of 1000 Hz (bandwidth: [1 100] Hz). SSVEPs were recorded using all 64 electrodes, which were placed according to the international standard 10-20 system. The reference electrode was located at the vertex. Electrode impedances were kept below 10 kΩ. Subjects were seated in a comfortable chair at a viewing distance of approximately 70 cm from the monitor in a dimly lit soundproof room.

2.3 Data analysis

The SSVEPs were calculated using the processing method of antiphase stimulation described in Ref. [11]. The envelopes of SSVEP were obtained by calculating the absolute value of a Hilbert transform, with an SSVEP bandpass frequency range of $f-3$ to $f+3$ (where f was the fundamental SSVEP frequency). The SSVEP envelope from -0.2 s to 1 s was treated as the object for modeling (Time 0 was the start time of SSVEP stimulation, which was marked with triggers). A paired t-test analysis was used to test the difference in fitting result between the four different models and the SSVEP envelope data, the results of the t-test analysis are expressed by t (df) and p, in which t was the test statistic; df was the degrees of freedom, and p reflected the statistical significance level. Statistical significance was defined as $p<0.05$.

2.4 Modeling

In order to study the dynamic process of SSVEP, four linear system models were used to quantitatively study the SSVEP envelope. The SSVEP envelope was considered as a low-order system for simplicity and to make it physically explicable. Considering the flashing stimulation envelope as a step stimuli, the linear system and response could be expressed by the following equation in the s-domain[32],

$$R(s)=E(s)\cdot H(s) \quad (2)$$

where we regarded $H(s)$ as a linear system being expressed as a transfer function in the s-domain. To make the dynamic model simple (with few parameters) and interpretable, only second-order (two poles) and third-order (three poles) linear systems were used to fit the SSVEP envelope. To verify the effect of the presence of a zero point on the fitting results, we also compared the two cases of whether the model has a zero point or not. Therefore, a total of 4 models were used in this study to fit the SSVEP envelope (second-order and third-order, with and without zero point). The transfer functions of the four linear models are shown in Table 1, the characteristics of which were a second-order system without zero point (Model 1), a second-order system with zero point (Model 2), a third-order system without zero point (Model 3), and a third-order system with zero point (Model 4). For the parameters of each system in Table 1, ζ is the damping coefficient, T_d is the response latency, T_ω is the natural period, T_z relates to the zero point, T_{p3} relates to the 3rd pole, and K is the static gain.

In this study, we mainly focused on the characteristics of SSVEP in the transient process. Given that the duration of the transient-state response is about 0.5 s, the SSVEP envelope from -0.2 s to 1 s (Time 0 was the start time of SSVEP stimulation, which was marked with triggers) was treated as the object of modeling, which included the whole transient-state process and some of the stable-state process.

Table 1 Transfer functions of different models.

Model	$H(s)$
1	$\dfrac{K\times \mathrm{e}^{-T_d s}}{1+(2\times\zeta\times T_\omega)s+T_\omega^2 s^2}$
2	$\dfrac{K(1+T_z s)\times \mathrm{e}^{-T_d s}}{1+(2\times\zeta\times T_\omega)s+T_\omega^2 s^2}$
3	$\dfrac{K\times \mathrm{e}^{-T_d s}}{1+(2\times\zeta\times T_\omega)s+T_\omega^2 s^2(1+T_{p3}s)}$
4	$\dfrac{K(1+T_z s)\times \mathrm{e}^{-T_d s}}{1+(2\times\zeta\times T_\omega)s+T_\omega^2 s^2(1+T_{p3}s)}$

3 Results

3.1 Validity of modeling

The modeling test was carried out in two phases: a Single-Subject (SS) test and a Multi Subject (MS) test. The SS test was conducted to analyze the SSVEP of each subject and to analyze the SSVEP envelope under different conditions, while the MS test was conducted to analyze the average SSVEP for all subjects and to verify the model and further confirm the validity of the SS test analysis. For the MS test, half of the trials were randomly selected to generate the SSVEP envelope as a working signal, while the remaining trials used to generate the SSVEP envelope as a validation signal. The working signal was used to generate the signal models and the validation data was used to verify the signal models.

The fitting accuracy was used to measure the fitting degree of the model to the data. The fitting accuracy was calculated by

$$\text{fit} = 1 - \frac{\|X - X_{\text{fit}}\|}{\|X - \text{mean}(X)\|} \tag{3}$$

where X represents the fitting object, X_{fit} represents the fitting result, and $\|\cdot\|$ represents the binary norm. Table 2 shows the fitting accuracies for different pre-stimulation conditions in the MS test. The results shown in Table 2 indicated that Model 4 had the highest average fitting accuracy and Model 3 had the lowest, regardless of the stimulus frequencys and types of pre-stimulation.

Corresponding to Table 2, Fig. 2 shows the temporal waveforms of the working signal, validation signal, and fitting signals under the four different models in the MS test. The waveform results indicated that in all stimulation frequency and pre-stimulation conditions, the four dynamic models returned good fitting results with both working signals and validation signals. Furthermore, differences remained in the fitting results of the four models: the fitting waveforms of Model 4 had the highest fitting effect with the working data, while Model 3 had the worst effect.

Figure 3 indicates the accuracy of fitting under different pre-stimulation conditions for the SS test. Pairwise comparisons showed that the fitting accuracy of Model 2 was significantly higher than that of Model 1 in the conditions of 15 Hz with white

Table 2 Accuracy of fitting under different conditions of validation data.

(%)

Pre-stimulation	15 Hz				9 Hz			
	Model 1	Model 2	Model 3	Model 4	Model 1	Model 2	Model 3	Model 4
Black	84.7	88.0	69.5	95.8	74.0	85.46	74.1	85.0
Gray	93.1	93.7	92.9	93.8	84.1	85.6	82.8	93.9
White	87.3	88.7	77.2	93.1	74.9	79.8	74.9	79.9
Average	88.3 ± 3.5	90.1 ± 2.6	79.9 ± 9.7	94.3 ± 1.2	78.0 ± 4.4	83.6 ± 2.7	77.3 ± 4.0	86.3 ± 5.8

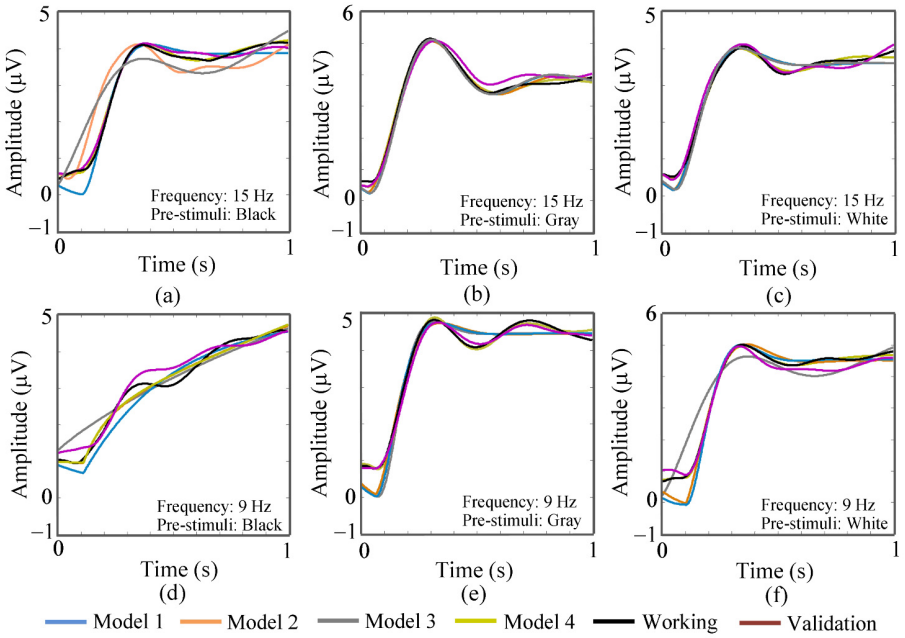

Fig. 2 Temporal waveform of working signal, validation signal, and the fitting signal under the four different models in MS test.

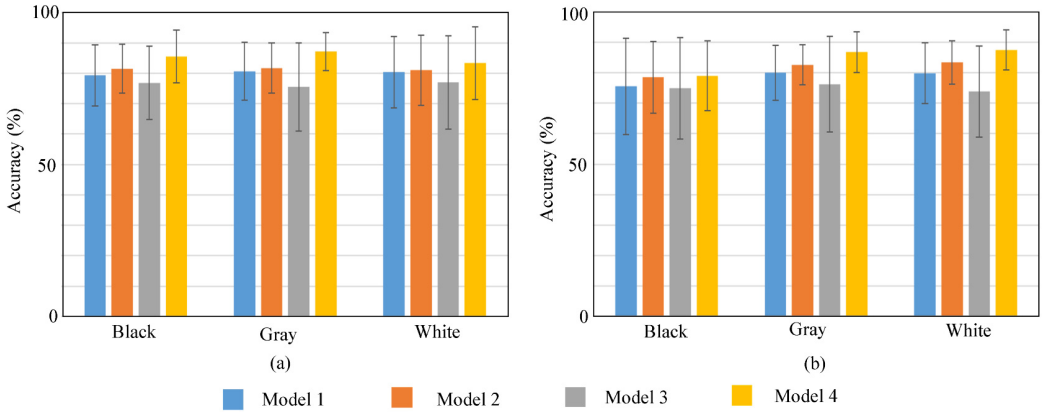

Fig. 3 Accuracy of fitting under different conditions of working data, (a) 15 Hz stimulation and (b) 9 Hz stimulation.

pre-stimulation ($t(13) = 1.878$, $p = 0.042$), 9 Hz with black pre-stimulation ($t(13) = 1.821$, $p = 0.046$), and 9 Hz with white pre-stimulation ($t(13) = 2.676$, $p < 0.01$); the fitting accuracy of Model 4 was significantly higher than that of Model 3 in the conditions of 15 Hz with black pre-stimulation ($t(13) = 2.614$, $p = 0.011$), 15 Hz with gray pre-stimulation ($t(13) = 2.798$, $p = 0.008$), 15 Hz with white pre-stimulation ($t(13) = 2.121$, $p = 0.027$), 9 Hz with gray pre-stimulation ($t(13) = 2.404$, $p = 0.016$), and 9 Hz with white pre-stimulation ($t(13) = 3.104$, $p = 0.004$); and the fitting accuracy of Model 4 was significantly higher than that of Model 2 in the conditions of 15 Hz with black pre-stimulation ($t(13) = 2.427$, $p = 0.015$), 15 Hz with gray pre-stimulation ($t(13) = 2.904$, $p = 0.006$), 15 Hz with white pre-stimulation ($t(13) = 2.194$, $p = 0.024$), 9 Hz with gray pre-stimulation ($t(13) = 2.702$, $p = 0.009$), and 9 Hz with white pre-stimulation ($t(13) = 2.695$, $p = 0.009$). The above results indicated that models with zero points had better fitting accuracy results than models without zero points, and the third-order model had better fitting accuracy than the second-order model for models with a zero point.

3.2 Zero-pole analysis under different pre-stimulation conditions

Figure 4 shows the zeros and poles distribution for the four different models for 15 Hz stimulation. The results

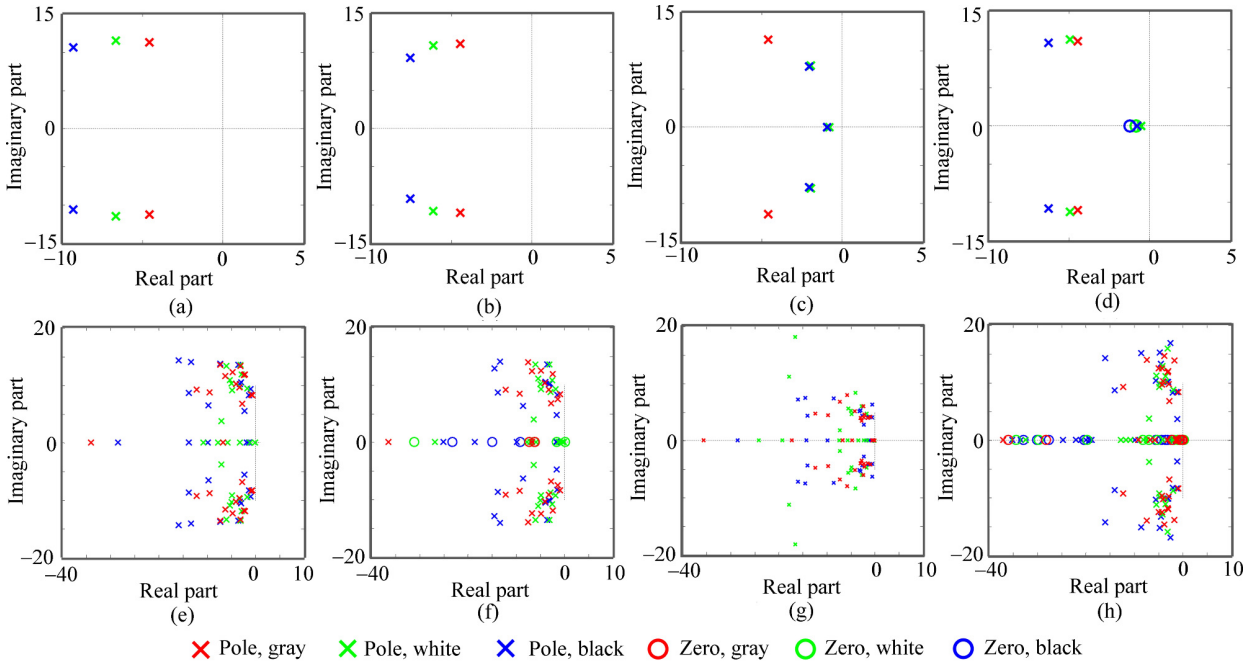

Fig. 4 Poles and zeros distribution (15 Hz). (a) and (e) Model 1; (b) and (f) Model 2; (c) and (g) Model 3; (d) and (h) Model 4; (a)–(d) zeros and poles by the averaged EEG of all subjects (MS test); (e)–(h) zeros and poles by the EEG of each subjects (SS test).

shown in Fig. 4 indicated that all of the poles were distributed in the left half plane of the s-domain. Poles comparison among models was the focus of this study. For the sake of uniformity, Fig. 4 only shows the zeros and poles from -10 to 5 (for the MS test) and from -40 to 10 (for the SS test) on the real coordinates. The zeros or poles far away from the imaginary axis were regarded as outliers and ignored for analysis.

The real coordinates of the conjugate poles were compared between different pre-stimulation conditions. The results of the MS test revealed that for Models 1, 2, and 4, the conjugated poles of the gray pre-stimulation condition were closest to the imaginary axis, followed by the white pre-stimulation condition and the black pre-stimulation condition: Model 1 (gray: -4.6, white: -6.7, black: -9.3), Model 2 (gray: -4.5, white: -6.2, black: -7.6), and Model 4 (gray: -4.5, white: -5.0, black: -6.3). In Model 3, the conjugate poles of the white pre-stimulation condition were closest to the imaginary axis, followed by the black pre-stimulation and the gray pre-stimulation: Model 3 (gray: -4.6, white: -2.0, black: -2.1). The ordinate differences of conjugate poles were also compared between different pre-stimulation conditions. In contrast to the real coordinates, for Models 1, 2, and 4, there was almost no significant difference in the imaginary coordinates of conjugate poles among different pre-stimuli conditions: Model 1 (gray: ± 11.3, white: ± 11.5, black: ± 10.6), Model 2 (gray: ± 11.0, white: ± 10.8, black: ± 9.3), and Model 4 (gray: ± 11.1, white: ± 11.3, black: ± 10.8). In Model 3, gray pre-stimulation returned significantly different results from black or white pre-stimulation (gray: ± 11.4, white: ± 8.0, black: ± 7.8).

In the MS test, the real coordinates of zeros were Model 2 (gray: -193.4, white: -93.5, black: -44.6) and Model 4 (gray: -134.6, white: -0.85, black: -1.22). The real coordinates of the third poles in the third-order models were Model 3 (gray: -464.6, white: -0.82, black: -0.94) and Model 4 (gray: -346.9, white: -0.54, black: -0.78).

Figure 5 shows the zeros and poles distribution for the four different models for the 9 Hz stimulation. All of the poles were distributed in the left half plane of the s-domain. Figure 5 only shows the zeros and poles from -20 to 5 (for the MS test) and from -40 to 10 (for the SS test) on the real coordinates, with the zeros or poles far away from the imaginary axis regarded as outliers.

The MS test results showed that the poles were all distributed on the real axis under 9 Hz black pre-stimulation condition, which was different from all other conditions in which conjugate poles were included. The real coordinates of conjugate poles between the pre-stimuli conditions of gray and white were close to each other in the MS test: Model 1 (gray: -10.0, white:

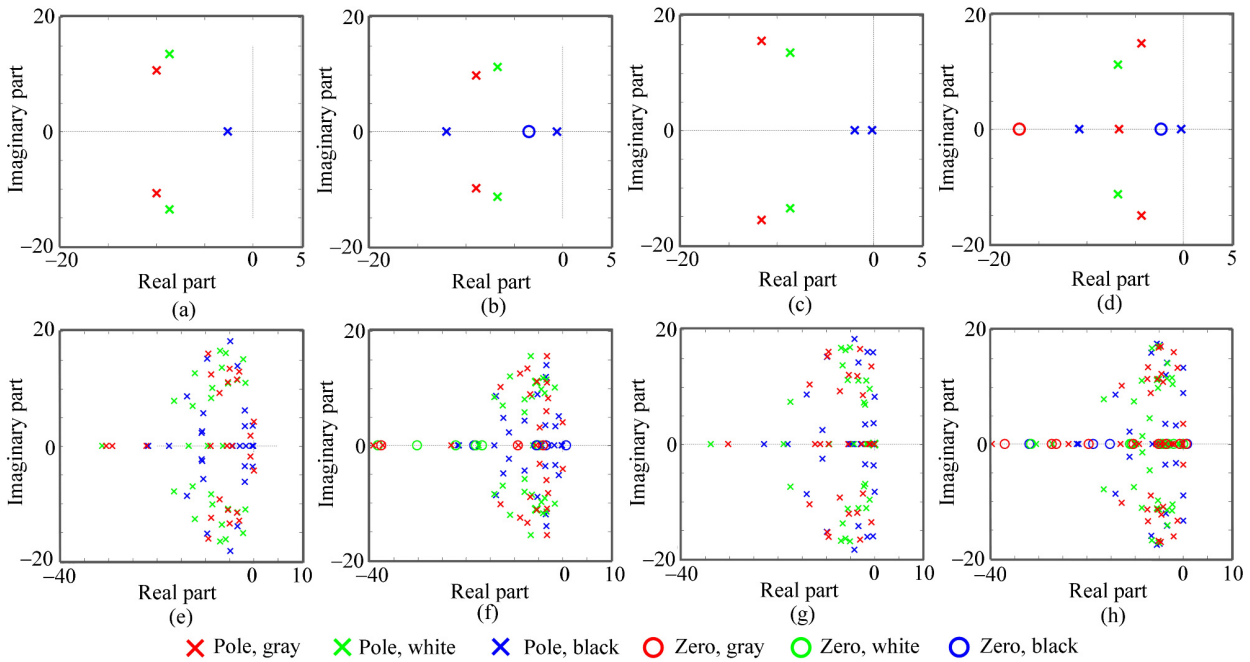

Fig. 5 Poles and zeros distribution (9 Hz). (a) and (e) Model 1; (b) and (f) Model 2; (c) and (g) Model 3; (d) and (h) Model 4; (a)–(d) zeros and poles by the averaged EEG of all subjects (MS test); (e)–(h) zeros and poles by the EEG of each subjects (SS test).

−8.6), Model 2 (gray: −8.9, white: −6.7), Model 3 (gray: −11.6, white: −8.7), and Model 4 (gray: −4.4, white: −6.8). The real coordinates of the poles related to the black pre-stimulation were −2.6 in Model 1, −0.5 and −12 in Model 2, −1.96 and −0.1 in Model 3, and −10.8 and −0.2 in Model 4, as shown in Figs. 5a–5d.

The ordinate difference of conjugate poles was also compared between different pre-stimulation conditions. Similarly to the real coordinates, the imaginary coordinates of conjugate poles between pre-stimuli conditions of gray and white were close to each other in the MS test: Model 1 (gray: −10.7, white: 13.57), Model 2 (gray: 9.89, white: 11.35), Model 3 (gray: 15.6, white: 13.6), and Model 4 (gray: 15.1, white: 11.4). The real coordinates of zeros were Model 2 (gray: −78.4, white: −34.7, black: −3.4) and Model 4 (gray: −17.0, white: −34.6, black: −2.3). The real coordinates of the third poles in the third-order models were Model 3 (gray: −24.3, white: −2642, black: −1271) and Model 4 (gray: −6.6, white: −2641, black: −1271).

4 Discussion

4.1 Effect of pre-stimulation conditions on the real axis coordinates of conjugate poles

The main purpose of the dynamic model analytical method in this paper was to address the limited attention previously paid to the SSVEP transient process and the lack of a quantitative analytical method. On the basis of Ref. [25], which showed that modeling was an effective analysis method for the SSVEP dynamic process. This study compared models with different orders and with and without zeros so as to further improve the fitting accuracy, and introduced the zero-pole analytical method to verify the effects of the pre-stimulation paradigm on SSVEP.

The results of the MS test showed that the 15 Hz conjugated poles of the gray pre-stimulation condition were the closest to the imaginary axis, followed by the white pre-stimulation condition and the black pre-stimulation condition in Models 1, 2, and 4. In fact, the above real axis coordinates of the conjugate poles represent the exact physical meaning.

It can be inferred from the second-order model formulas that there was a negative correlation between the real coordinates of the conjugate poles and the damping coefficient. Taking the second-order system as an example, the conjugate poles were the solution of

$$\frac{1}{T_\omega^2}+2\cdot\frac{\zeta}{T_\omega}+s^2=0 \tag{4}$$

so the real coordinates of the conjugate poles is $-\zeta/T_\omega$, which is a negative correlation with the damping coefficient ζ.

The results obtained in this study by using the zero-pole analytical method are reasonable and consistent with the results obtained in Ref. [25] by using the method of model parameters analysis. They both showed that under the 15 Hz stimulus, the gray pre-stimulation condition corresponded to the minimum damping coefficient, followed by the white and black pre-stimulation conditions. The results were similarly consistent with those in Ref. [25] under the 9 Hz stimulus. Both the zero-pole analytical method and the parameter analytical method can reflect relevant SSVEP characteristics, such as the damping coefficient. The zero-pole characteristics demonstrated that the gray pre-stimulation condition at 15 Hz and the white pre-stimulation condition at 9 Hz had the minimum damping coefficient. The pre-stimulation paradigm can affect SSVEP characteristics, and thus could be used in the improvement of SSVEP-BCI performance.

4.2 Effect of pre-stimulation conditions on the imaginary axis coordinate of conjugate poles

The theory on the characteristics of the conjugated poles in the s-domain states that the imaginary part of the poles, which is called the oscillation frequency, determines the frequency of the oscillation: the further it is from the real axis, the faster the oscillation is. If the imaginary part of the poles is zero, the response does not oscillate[33, 34].

In the case of the 15 Hz stimulus, the imaginary coordinates of the conjugate poles corresponding to the three pre-stimulation conditions were close to each other (see Figs. 4a–4d), which indicated that the SSVEP envelopes corresponding to the three forms of pre-stimulation had approximately similar oscillation frequencies (see Figs. 2a–2c). Similarly in the case of the 9 Hz stimulus, the conjugated poles corresponding to white and gray pre-stimulation conditions have a similar ordinate of conjugated poles (Fig. 5), and the corresponding SSVEP envelopes had approximately similar oscillation frequencies (Figs. 2e and 2f).

Different from other conditions, the poles corresponding to the black pre-stimulation condition of 9 Hz stimulation frequency are distributed on the real axis. The results indicated that the corresponding

SSVEP envelope did not oscillate and belonged to an over-damped time domain waveform, as shown in Fig. 2d. These conclusions are also consistent with those in Ref. [25], in which the natural frequency was the parameter determining the dynamic response time of the SSVEP envelope[35]: the higher the natural frequency is, the faster the SSVEP envelope responses. Reference [25] indicated no significant difference in natural frequency between the three pre-stimulation conditions or between the two stimuli frequencies. The average value was around 12 rad/s, which might be related to the natural frequency of the contraction of pupil facing light excitation. In this study, the imaginary part of the conjugate poles was used to reflect the frequency of the SSVEP envelope oscillation according to the theory of pole characteristics. The imaginary values did not show any significant difference between the three forms of pre-stimulation or between the two stimuli frequencies, which is consistent with Ref. [25]. There was a correlation between the natural frequency and the oscillation frequency. For example, in the second-order systems, the relationship between natural frequency equation and oscillation frequency f could be described as

$$\omega^2 = f^2 + \alpha^2 \tag{5}$$

in which α was the attenuation factor (the real part of the conjugate poles).

4.3 Effect of zeros on the systems

In this study, the zero-containing systems had better fitting accuracies than the zero-free systems, both for the second-order (increasing from 78.0 ± 4.4 to 83.6 ± 2.7 for 9 Hz, and from 88.3 ± 3.5 to 90.1 ± 2.6 for 15 Hz) and third-order systems (increasing from 77.3 ± 4.0 to 86.3 ± 5.8 for 9 Hz, and from 79.9 ± 9.7 to 94.3 ± 1.2 for 15 Hz). The results were consistent with the characteristic of the theory of zero pole analysis that increasing a zero can increase the stability of the system[26, 28]. When the zero point is added to the left plane of the s-domain, the overshoot of system response will increase, the bandwidth will increase, and the system adjustment time will reduce[36].

From the results, it seems that the closer the zero point was to the imaginary axis, the greater the improvement of the fitting accuracy of the zero point system, compared with the zero-free system. For example, for the second-order systems at 15 Hz, the real coordinates of zeros were (gray: -193.4, white: -93.5, black: -44.6) in Model 2 and, when compared with Model 1, the improvement of fitting accuracy from small to large was 0.6% for gray (from 93.1% to 93.7%), 1.4% for white (from 87.3% to 88.7%), and 3.3% for black (from 84.7% to 88.0%). The same conclusion can be drawn from the 9 Hz stimulus condition. Similarly, in the third-order systems, the gray pre-stimulus corresponded to the largest distance between the zero point and the imaginary axis, and the minimum improvement of fitting accuracy (0.9%) for the 15 Hz stimulus, while the white pre-stimulus corresponded to the lowest zero abscissa, and the minimum improvement of fitting accuracy (5%) for the 9 Hz stimulus.

The above results are consistent with the theory of the zero-pole characteristic that the closer the zero to the imaginary axis, the greater the influence on the system. When the real part of the zero point is much larger than the damping coefficient of the second-order system, the influence of the additional zero to the system is reduced, such that the influence of the zero point on the system can be ignored when the zero point is far from the imaginary axis.

4.4 Significance of the zero-pole analytical method in this study

In this study, four dynamic models were used to fit the SSVEP envelope, and the influence of pre-stimulation on the SSVEP envelope was determined by zero-pole analysis. The results given in this paper indicated that the characteristics of SSVEP could be drawn by the zero-pole analytical method as well as the parameter analytical method in Ref. [25]. The corresponding relationships between the zero-pole characteristics and the SSVEP characteristics have been obtained in the analysis presented in this paper. The real coordinates of the conjugate pole on the left plane of the s-domain was related to the damping coefficient. The imaginary coordinates of poles reflected the approximate oscillation frequency of the SSVEP envelope corresponding to the various pre-stimulation conditions. Zeros could improve the fitting accuracy of the model to the SSVEP envelopes, and the level of improvement was reflected by the zero point position.

The results of this study are consistent with Ref. [25], which reflects the reliability of the zero-pole analytical method presented in this paper. More importantly, the zero-pole analytical method reflects the stability of the dynamic model and provides a more intuitive analytical method for SSVEP characteristics. In Ref. [25], the SSVEP characteristics were analyzed by the modeling

parameters of a second-order system. The increase of zeros or poles, although it might improve the fitting accuracy, would introduce more parameters to the model and lead to difficulty in the interpretability of the model parameters. However, the zero-pole analytical method interprets the signal property by the zero-pole characteristic and avoids the interpretation problems of model parameters. The zero-pole analytical method provides a new method for signal characteristics analysis, and achieves a combination of a high fitting accuracy and easy interpretability.

The zero-pole analysis method has the potential to be used in the improvement of SSVEP-BCI performance, reflecting the characteristics of SSVEP[37]. Different from the parameter analytical method, which describes the envelope response, the zero-pole analytical method is a channel evaluation method. Therefore, we can transform the model into a minimum phase system and achieve channel enhancement through filtering or other methods.

The results shown in this paper therefore have the potential to be applied to SSVEP-BCIs. For example, the zero-pole analytical method showed that the gray pre-stimulation condition resulted in the smallest damping coefficient of the SSVEP dynamic model and the largest SSVEP amplitudes, which indicates its potential to enhance SSVEP-BCI performance compared with the black and white conditions. Due to energy limitations, the conclusions of this paper were based on SSVEP data induced by a single flicker. However, the conclusions of this study on the effect of pre-stimulation on SSVEP were still meaningful and have the potential to be used in SSVEP-BCIs. The experimental results of this paper might be extended to the multi-objective stimulus paradigm, although this needs to be verified by further study.

5 Conclusion

In this paper, we explored the effectiveness of modeling methods for the study of SSVEP characteristics and evaluated the effect of the pre-stimulation method on SSVEP based on zero-pole characteristics. The fitting accuracy results based on three kinds of pre-stimulation methods and four kinds of dynamic models showed the effectiveness of the modeling method and the effect of model order and zero points. More importantly, it was found that the damping coefficient and other characteristics of SSVEP envelopes could be reflected in the characteristics of zero-pole, thus indicating that the zero-pole analytical method is an effective tool for the evaluation of SSVEP characteristics. The effect of pre-stimulation on SSVEP characteristics was analyzed by comparing zero-pole characteristics between different pre-stimulation conditions. Among the three pre-stimulation conditions (black, gray, and white), the gray condition was shown to be the most likely to improve the performance of SSVEP-BCI due to its correspondence with the smallest damping coefficient. The zero-pole analysis modeling method achieves a combination of high fitting accuracy and easy interpretability, and has unique advantages for the quantitative study of SSVEP characteristics.

Acknowledgment

This work was supported by the Key Research and Development Program of Guangdong Province (No. 2018B030339001); the National Key Research and Development Program of China (No. 2017YFB1002505), and the National Natural Science Foundation of China (No. 61431007).

References

[1] X. G. Chen, Z. K. Chen, S. K. Gao, and X. R. Gao, Brain-computer interface based on intermodulation frequency, *J. Neural. Eng.,* vol. 10, no. 6, p. 066009, 2013.

[2] K. Lin, S. K. Gao, and X. R. Gao, Boosting the information transfer rate of an SSVEP-BCI system using maximal-phase-locking value and minimal-distance spatial filter banks, *Tsinghua Science and Technology,* vol. 24, no. 3, pp. 262–270, 2019.

[3] J. J. Chen, D. Zhang, A. K. Engel, Q. Gong, and A. Maye, Application of a single-flicker online SSVEP BCI for spatial navigation, *Plos One,* vol. 12, no. 5, p. e0178385, 2017.

[4] X. G. Chen, Y. J. Wang, S. G. Zhang, S. K. Gao, Y. Hu, and X. R. Gao, A novel stimulation method for multi-class SSVEP-BCI using intermodulation frequencies, *J. Neural. Eng.,* vol. 14, no. 2, p. 026013, 2017.

[5] W. C. Zhang, F. C. Sun, H. Wu, C. Q. Tan, and Y. Z. Ma, Asynchronous brain-computer interface shared control of robotic grasping, *Tsinghua Science and Technology,* vol. 24, no. 3, pp. 360–370, 2019.

[6] W. C. Zhang, C. Q. Tan, F. C. Sun, H. Wu, and B. Zhang, A review of EEG-based brain-computer interface systems design, *Brain Science Advances,* vol. 4, no. 2, pp. 156–167, 2018.

[7] K. Servick, Computers turn neural signals into speech, *Science,* vol. 363, no. 6422, p. 14, 2019.

[8] X. P. Si, W. J. Zhou, and B. Hong, Neural distance amplification of lexical tone in human auditory cortex, in *Proc. 36th Annual International Conference of the IEEE Engineering in Medicine and Biology Society (EMBC)*, Chicago, IL, USA, 2014, pp. 4001–4004.

[9] X. P. Si, W. J. Zhou, and B. Hong, Cooperative cortical network for categorical processing of Chinese lexical tone, *Proceedings of the National Academy of Sciences of the United States of America*, vol. 114, no. 46, pp. 12 303–12 308, 2017.

[10] G. Y. Bin, X. R. Gao, Z. Yan, B. Hong, and S. K. Gao, An online multi-channel SSVEP-based brain-computer interface using a canonical correlation analysis method, *J. Neural. Eng.,* vol. 6, no. 4, p. 046002, 2009.

[11] X. G. Chen, Y. J. Wang, M. Nakanishi, X. R. Gao, T. P. Jung, and S. K. Gao, High-speed spelling with a noninvasive brain-computer interface, *Proceedings of the National Academy of Sciences of the United States of America*, vol. 112, no. 44, pp. E6058–E6067, 2015.

[12] S. K. Gao, Y. J. Wang, X. R. Gao, and B. Hong, Visual and auditory brain-computer interfaces, *IEEE Transactions on Biomedical Engineering*, vol. 61, no. 5, pp. 1436–1447, 2014.

[13] D. Regan, *Human Brain Electrophysiology: Evoked Potentials and Evoked Magnetic Fields in Science and Medicine*. New York, NY, USA: Elsevier, 1989.

[14] C. S. Herrmann, Human EEG responses to 1–100 Hz flicker: Resonance phenomena in visual cortex and their potential correlation to cognitive phenomena, *Experimental Brain Research*, vol. 137, nos. 3&4, pp. 346–353, 2001.

[15] P. J. Kohler, W. J. Meredith, and A. M. Norcia, Revisiting the functional significance of binocular cues for perceiving motion-in-depth, *Nature Communications*, vol. 9, no. 1, p. 3511, 2018.

[16] M. S. Livingstone and D. H. Hubel, Psychophysical evidence for separate channels for the perception of form, color, movement, and depth, *Journal of Neuroscience*, vol. 7, no. 11, pp. 3416–3468, 1987.

[17] W. Q. Yan, G. H. Xu, J. Xie, M. Li, S. C. Zhang, and A. L. Luo, Study on the effects of brightness contrast on steady-state motion visual evoked potential, in *Proc. 39th Annual International Conference of the IEEE Engineering in Medicine and Biology Society (EMBC)*, Jeju Island, Korea, 2017, pp. 2263–2266.

[18] V. Zemon and J. Gordon, Luminance-contrast mechanisms in humans: Visual evoked potentials and a nonlinear model, *Vision Research*, vol. 46, no. 24, pp. 4163–4180, 2006.

[19] D. Regan, Some characteristics of average steady-state and transient responses evoked by modulated light, *Electroencephalography and Clinical Neurophysiology*, vol. 20, no. 3, pp. 238–248, 1966.

[20] D. Regan, Recent advances in electrical recording from the human brain, *Nature*, vol. 253, no. 5491, pp. 401–407, 1975.

[21] L. H. van der Tweel and H. Spekreijse, Signal transport and rectification in the human evoked-response system, *Annals of the New York Academy of Sciences*, vol. 156, no. 2, pp. 678–695, 1969.

[22] D. Regan, Some early uses of evoked brain responses in investigations of human visual function, *Vision Research*, vol. 49, no. 9, pp. 882–897, 2009.

[23] G. G. Celesia, Steady-state and transient visual evoked-potentials in clinical-practice, *Annals of the New York Acadmy of Sciences*, vol. 388, no. Jun, pp. 290–305, 1982.

[24] K. Smigasiewicz, M. Liebrand, J. Landmesser, and R. Verleger, How handedness influences perceptual and attentional processes during rapid serial visual presentation, *Neuropsychologia*, vol. 100, pp. 155–163, 2017.

[25] S. G. Zhang, X. Han, X. G. Chen, Y. J. Wang, S. K. Gao, and X. R. Gao, A study on dynamic model of steady-state visual evoked potentials, *J. Neural. Eng.,* vol. 15, no. 4, p. 046010, 2018.

[26] S. Haykin, B. V. Veen, and S. Haykin, *Signals and Systems (Second Edition)*. Beijing, China: Publishing House of Electronics Industry, 2012.

[27] A. V. Oppenheim and G. C. Verghes, *Signals, Systems and Inference*. Beijing, China: China Machine Press, 2017.

[28] C. L. Phillips, *Signals, Systems and Transforms (Fourth Edition)*. Beijing, China: China Machine Press, 2009.

[29] M. A. Pastor, J. Artieda, J. Arbizu, M. Valencia, and J. C. Masdeu, Human cerebral activation during steady-state visual-evoked responses, *Journal of Neuroscience*, vol. 23, no. 37, pp. 11 621–11 627, 2003.

[30] X. Chen, Z. Chen, S. Gao, and X. Gao, A high-ITR SSVEP-based BCI speller, *Brain-Computer Interfaces*, vol. 1, nos. 3&4, pp. 181–191, 2014.

[31] N. V. Manyakov, N. Chumerin, A. Robben, A. Combaz, M. van Vliet, and M. M. van Hulle, Sampled sinusoidal stimulation profile and multichannel fuzzy logic classification for monitor-based phase-coded SSVEP brain-computer interfacing, *J. Neural. Eng.,* vol. 10, no. 3, p. 036011, 2013.

[32] B. Wu, S. Yang, and A. Huang, *Fundamentals of Mechanical Control Engineering*. Wuhan, China: Wuhan University of Technology Press, 2004.

[33] A. V. Oppenheim and R. W. Schafer, *Discrete-Time Signal Processing (Third Edition)*. Beijing, China: Publishing House of Electronics Industry, 2011.

[34] R. G. Lyons, *Understanding Digital Signal Processing (Third Edition)*. Beijing, China: Publishing House of Electronics Industry, 2012.

[35] B. Johansson and P. Jakobsson, Fourier analysis of steady-state visual evoked potentials in subjects with normal and defective stereo vision, *Documenta Ophthalmologica*, vol. 101, no. 3, pp. 233–246, 2001

[36] E. W. Kamen and B. S. Heck, *Fundamentals of Signals and Systems Using the Web and Matlab (Third Edition)*. Beijing, China: Science Press, 2016.

[37] S. G. Zhang and X. R. Gao, The effect of visual stimuli noise and fatigue on steady-state visual evoked potentials, *J. Neural. Eng.,* doi:10.1088/1741-2552/ab1f4e.

Shangen Zhang received the BEng degree from the University of Electronic Science and Technology of China in 2007, and the PhD degree from Tsinghua University in 2019. His research interests focus on brain-computer interface, biomedical signal processing, and machine learning.

Xu Han received the BS degree from Huazhong University of Science and Technology in 2016, and the MS degree from Tsinghua University in 2019. He is currently a master student at the Department of Biomedical Engineering, Tsinghua University. His research interests focus on biomedical signal processing, brain-computer interface, biomedical signal processing, and machine learning.

Xiaorong Gao received the BS degree from Zhejiang University in 1986, the MS degree from Peking Union Medical College in 1989, and the PhD degree from Tsinghua University in 1992. He is currently a professor of the Department of Biomedical Engineering, Tsinghua University. His current research interests are biomedical signal processing and medical instrumentation, especially the study of brain-computer interface.